J. Fluid Mech. (2002), *vol.* 467, *pp.* 101–127. © 2002 Cambridge University Press
DOI: 10.1017/S002211200200126X Printed in the United Kingdom

Self-propelling slugs

By JOSÉ BICO[1] AND DAVID QUÉRÉ[2]

[1]Department of Mechanical Engineering, Massachusetts Institute of Technology, Cambridge, Massachusetts 02139, USA

[2] Laboratoire de Physique de la Matière Condensée, UMR 7125 du CNRS, Collège de France, 75231 Paris Cedex 05, France

(Received 12 November 2001 and in revised form 6 February 2002)

Surface coating is generally achieved by an active operation: painting with a brush; withdrawing from a bath. Porous imbibition constitutes a more passive way: a porous material just put in contact with a reservoir containing a wetting fluid is spontaneously invaded. In this case, the material can eventually be filled by the fluid. If the aim is to coat only the surface of the pores, the liquid excess must be actively removed. We present an experiment in which a liquid train spontaneously moves in a capillary tube because of the trail it leaves behind. From a practical point of view, this system achieves a coating of the tube. The condition required for this motion and a model for its dynamics are presented. We also show how these trains can drive extremely viscous liquid slugs (or even solid bodies) in narrow tubes. We discuss the thickness of the deposited films. Extensions and limits of this system in more complex geometries are finally described, together with special cases such as the deposition of solid films.

1. Introduction

The motion of a fluid in a tube is generally forced by an external field, such as gravity or a pressure force. Here, we are interested in cases where the liquid moves in the absence of such a field, because of surface forces. The most classical example of such a motion, of great historical importance, is the capillary rise, or capillary flow (figure 1*a*). A tube connected with a reservoir of wetting liquid is invaded by this liquid, up to the point where gravity balances the capillary force. The driving force can be related to the existence of a meniscus at the front of the column which develops in the tube, and the motion can be represented as resulting from an asymmetry between the front and the rear of the column. It is tempting to generalize this proposition, and indeed different situations were reported in the literature where the motion of an index in a tube was found to be the result of an asymmetry.

A slug placed in an open conical tube moves up to the tip of the cone (Bouasse 1924), because of the difference in Laplace pressure between both menisci (figure 1*b*). Weislogel (1997) considered a tube, treated to be successively hydrophilic and hydrophobic (figure 1*c*). As the liquid preferentially wets the hydrophilic part, a slug placed across the frontier runs away from the hydrophobic side. The motion stops when the whole slug is in the hydrophilic side. A dynamic version of this idea is the chemically reactive drop developed by Bain, Burnett-Hall & Montgomerie (1994) and Domingues dos Santos & Ondarçuhu (1995). The liquid contains surface reactive molecules such as chlorosilanes, which modify the wettability of the solid when they are grafted onto it. Thus, if the reaction starts on one side of the drop, the tube

https://doi.org/10.1017/S002211200200126X Published online by Cambridge University Press

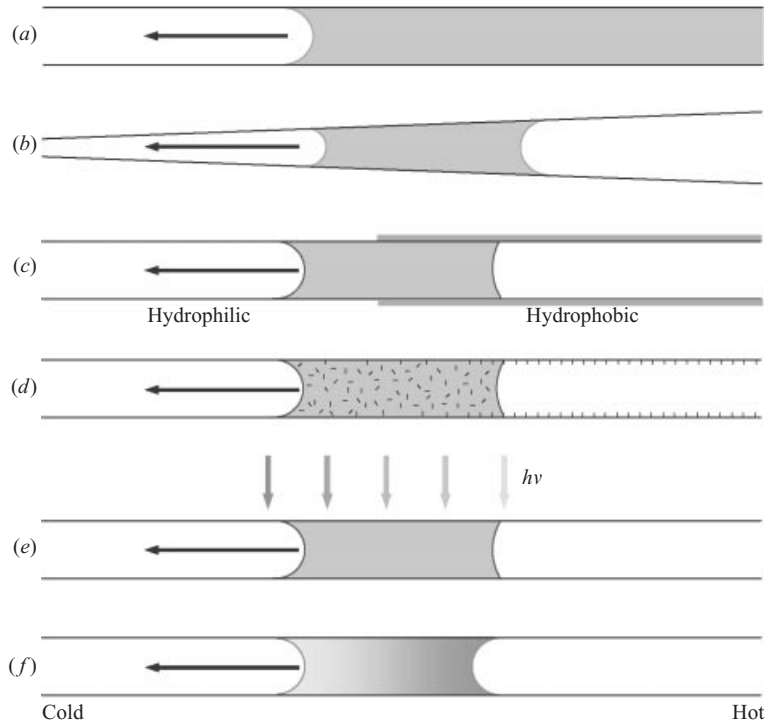


FIGURE 1. Asymmetric spontaneous moving slugs in a tube. (*a*) Capillary imbibition. (*b*) Conical tube. (*c*) Chemically asymmetric tube. (*d*) Liquid containing a reactive surfactant. (*e*) Photosensitive surface. (*f*) Thermocapillary motion.

becomes asymmetric, which implies a motion (de Gennes 1998), whose effect is to maintain this asymmetry (figure 1*d*).

Situations implying an external action were also described recently. For example, photosensitive systems have been produced (Ichimura, Oh & Nakagawa 2000) where the tube wall is coated with a compound, whose surface energy changes when exposed to the light. A gradual lighting then induces the motion of a liquid index (figure 1*e*). Thermocapillary motion can also drive a liquid with a surface (Mazouchi & Homsy 2000). Since the surface tension of a liquid usually decreases with a rise of its temperature, a liquid index can run away from the heated end of a capillary tube (figure 1*f*).

In the system studied here, the asymmetry is forced by juxtaposing two drops inside a tube (figure 2); we call this device a *bislug*. If both liquids wet the tube, the forces at the meniscus do not compensate, which induces a motion, first reported by Marangoni (1871) for a system of water–carbon disulfide. Bico & Quéré (2000) discussed the driving force of this train, and measured its velocity in two cases: (i) when the viscosities of both liquids are the same; (ii) when the first liquid is much less viscous than the second, and thus can be used as a lubricant for the motion.

Such a bislug is pictured in figure 2. It leaves behind two superposed films, and thus is slowly consumed during its displacement. If it reaches the end of the tube before being exhausted, the experiment is reproducible by inclining the tube in order to drive the bislug back. We first identify the driving force of the system. Then, we focus on the dynamics and discuss the bislug velocity in different limits, and incorporate

https://doi.org/10.1017/S002211200200126X Published online by Cambridge University Press

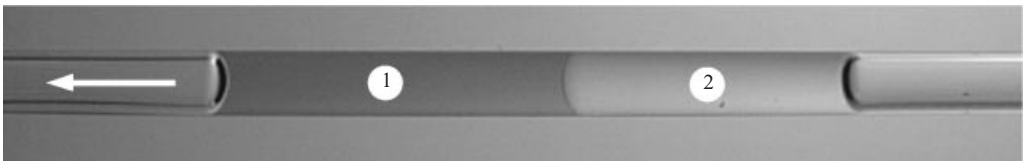


FIGURE 2. A bislug composed of two wetting liquids spontaneously moves in a tube. Here, the liquids are ethylene glycol and silicone oil, and they are juxtaposed in a glass capillary tube of millimetric diameter.

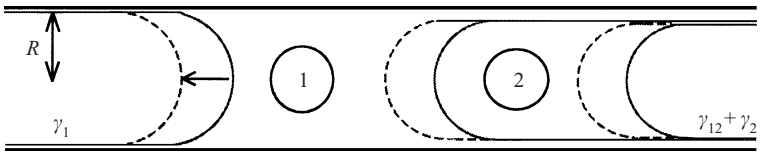


FIGURE 3. Small displacement of a bislug: two interfaces liquid 2/air and liquid 1/liquid 2 replace a liquid 1/air interface.

local dissipations to understand the data quantitatively. We also specify the laws of deposition, both for the first film (left by the first liquid) and for the second film (deposited on the first film). Finally, we describe special cases, in particular, situations where the liquids are miscible, or even reactive towards each other, and possible extensions to other geometries.

2. Driving force

2.1. *Prewetted tubes*

In the example of figure 2 (ethylene glycol/silicone oil in a glass tube), the motion is observed to be in the direction of the arrow. The bislug has three menisci, all in a wetting situation, and the middle one faces the rear of the bislug. In addition, we consider that the tube was first prewetted by liquid 1. Then, the driving force can be deduced from simple energy arguments; when the bislug moves, an interface liquid 1/air is changed into two interfaces liquid 2/air and liquid 1/liquid 2 (figure 3).

An infinitesimal displacement of the bislug implies a change of energy:

$$\mathrm{d}E = 2\pi R(\gamma_2 + \gamma_{12} - \gamma_1)\,\mathrm{d}x, \tag{1}$$

where R is the tube radius, γ_1 and γ_2 are the surface tensions of liquids 1 and 2 and γ_{12} is the interfacial tension between liquids 1 and 2. The force is then given by:

$$F = -\frac{\mathrm{d}E}{\mathrm{d}x} = 2\pi R\Delta\gamma \quad \text{with} \quad \Delta\gamma = \gamma_1 - \gamma_{12} - \gamma_2. \tag{2}$$

Hence, the driving force is found to be related mainly to the contrast in surface tensions between both liquids (corrected by the small intermediate surface tension). This justifies the use of the convenient metaphors of the *locomotive* (which drives the train) for the first liquid, and the *waggon* (which induces a force opposing the motion) for the second one, even if here, contrary to normal trains, the waggon is necessary for the motion.

The same arguments can be used for *multislugs* systems. A bislug can also move in an immersed environment, in water for example. The main difficulty is to find two immiscible liquids which do not mix in water. A bislug composed of perfluorodecalin and ethyl acetate in a Teflon tube filled with water is an example of such a system.

https://doi.org/10.1017/S002211200200126X Published online by Cambridge University Press

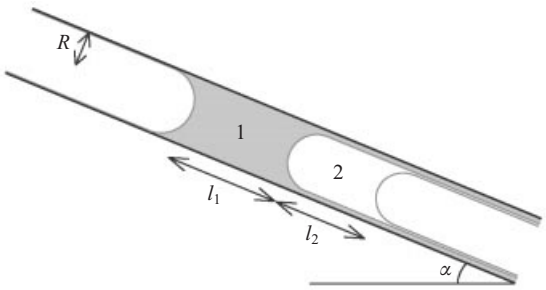


FIGURE 4. Direct measurement of the driving force. When gravity balances the capillary force, the bislug stops.

The driving force may also be deduced from the Laplace law, the pressure difference between the front and the rear meniscus being the sum of three Laplace pressure jumps:

$$\Delta P = \frac{2(\gamma_1 - \gamma_{12} - \gamma_2)}{R} = \frac{2\Delta\gamma}{R}. \tag{3}$$

If we multiply this pressure by the tube section, we again obtain equation (2).

Interfacial tensions were measured experimentally with the classical ring method, giving for the system ethylene glycol/silicone oil: $\gamma_1 = 47.7 \pm 0.1\,\mathrm{mN\,m^{-1}}$, $\gamma_2 = 20.3 \pm 0.1\,\mathrm{mN\,m^{-1}}$ and $\gamma_{12} = 18.0 \pm 0.2\,\mathrm{mN\,m^{-1}}$. Hence, the driving interfacial tension is $\Delta\gamma = 9.3 \pm 0.4\,\mathrm{mN\,m^{-1}}$. The driving force can also be measured directly by inclining the tube until the bislug stops. Then, gravity balances the capillary force (figure 4), which can be written:

$$F = \pi R^2(\rho_1 l_1 + \rho_2 l_2)\mathrm{g}\sin\alpha, \tag{4}$$

where α is the tilting angle for which the motion stops, ρ_1 and ρ_2 the liquid densities, and l_1 and l_2 the lengths of the successive indices composing the train.

We present in figure 5 typical measurements of α, for an ethylene glycol/silicone oil system in a glass capillary tube of radius $R = 511\,\mu\mathrm{m}$. The densities are, respectively, 1.11 and 0.95 and the total length of the slug can be varied, typically in the centimetre range. This plot is linear, as expected from equation (4), and the slope of this line gives the force per unit length. For this particular example, we find that $F/2\pi R = 10.0 \pm 0.3\,\mathrm{mN\,m^{-1}}$, in close agreement with the value determined by tensiometry ($\Delta\gamma = 9.3 \pm 0.4\,\mathrm{mN\,m^{-1}}$).

2.2. *Dry tubes*

In the previous experiments, the capillary tube was first prewetted by liquid 1. In a dry tube, a small displacement $\mathrm{d}x$ of the train implies a change of surface energies:

$$\mathrm{d}E = 2\pi R(\gamma_2 + \gamma_{12} + \gamma_{SL} - \gamma_{SV})\,\mathrm{d}x, \tag{5}$$

where γ_{SL} and γ_{SV} are the solid/liquid 1 and solid/air interfacial tensions. However, the expression of the driving force should not change and remains as given by (2), as if the tube were prewetted. This is reminiscent of what happens in capillary rise; there, the driving force is given by the difference in surface tension between the dry tube and the wet tube, namely $(\gamma_{SV} - \gamma_{SL})$. The latter quantity is not bounded *a priori*, whereas the height of the capillary rise is, at a value which is proportional to γ, the liquid/vapour surface tension. In a wetting situation, $(\gamma_{SV} - \gamma_{SL})$ can be larger than γ so that it is energetically favourable for a film to develop ahead of the meniscus.

https://doi.org/10.1017/S0022112002001260X Published online by Cambridge University Press

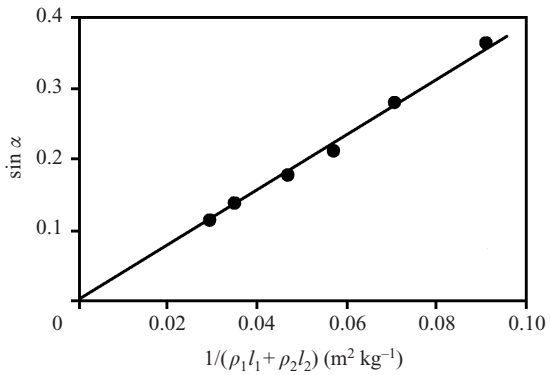


FIGURE 5. Sinus of the measured equilibrium tilting angle versus the inverse of the quantity $\rho_1 l_1 + \rho_2 l_2$. The system is an ethylene glycol/silicone oil bislug in a glass tube of radius 511 μm.

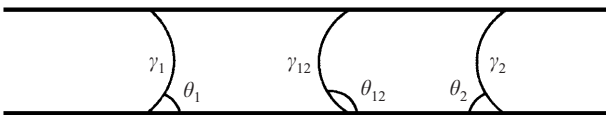


FIGURE 6. Partial wetting case: the train does not move.

Thus, the advancing meniscus progresses on a microscopic precursor film. De Gennes (1985) has shown that the energy excess per unit surface ($\gamma_{SV} - \gamma_{SL} - \gamma$) is exactly consumed in the progression of this precursor film.

These arguments are valid for a bislug moving on a dry surface. In a complete wetting situation, a microscopic film develops ahead of the front meniscus, which progresses on this film. Thus, the driving force $\Delta\gamma$ is the same as in the prewetted case, and is still given by equation (2) (we checked this point experimentally, using the tilting method for measuring $\Delta\gamma$ for a dry system, and for a prewetted one). As a consequence, these forces are always measurable, since they only involve tensions between a liquid and a vapour and between two liquids.

2.3. *Partial wetting*

In the case of partial wetting for the three menisci, the Laplace force can be written:

$$F = 2\pi R\,(\gamma_1 \cos\theta_1 - \gamma_{12}\cos\theta_{12} - \gamma_2 \cos\theta_2), \tag{6}$$

where θ_1, θ_{12} and θ_2 are the contact angle at each meniscus (figure 6). The Young relation relates the contact angle and the interfacial tensions:

$$\gamma_{ij}\cos\theta_{ij} = \gamma_{Si} - \gamma_{Sj}. \tag{7}$$

Then, the force F can be calculated. All the terms cancel, and we find that $F = 0$. This result can be understood simply in terms of surface energies; in partial wetting, the displacement of the train does not induce any coating, and thus surface energies remain unchanged. Thus, there is no reason for the train to move. More generally, a necessary condition for observing a spontaneous motion is that one meniscus (at least) must be completely wetting.

2.4. *Middle meniscus*

In the system considered in figure 2, the middle meniscus was curved towards liquid 2, and thus opposed the motion. If the two liquids are hydrophilic/hydrophobic (the

https://doi.org/10.1017/S002211200200126X Published online by Cambridge University Press

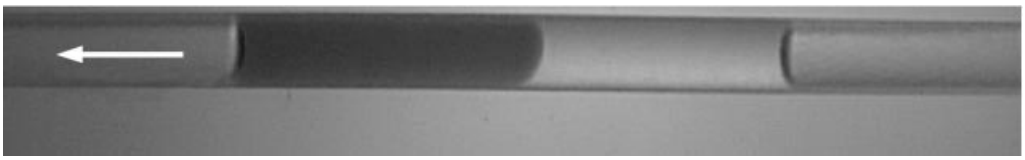


FIGURE 7. Inverted middle meniscus: ethanol/silicone oil bislug in a polyethylene tube.

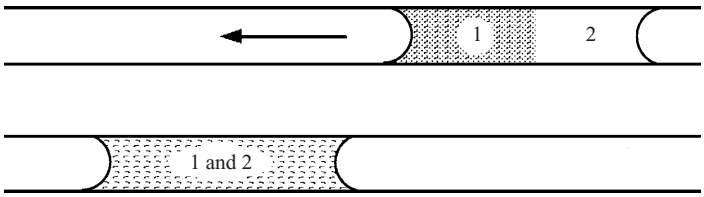


FIGURE 8. Bislug prepared with two miscible liquids (with $\gamma_1 > \gamma_2$). As long as the liquids are not totally mixed, the slug moves.

most common case), this implies a hydrophilic solid (which was the case in figure 2, where the tube was made of glass). Taking a hydrophobic tube (made of polymer, for example) leads to the opposite case, but the liquids must still wet the material. The latter condition can be rather restricting with a low-energy surface, which, in practice, makes this situation rarer. A bislug prepared with ethanol and silicone oil in a polyethylene tube is an example of this kind of system (figure 7). In this case, the middle meniscus also drives the liquid and the force per unit length can be written:

$$\Delta\gamma = \gamma_1 + \gamma_{12} - \gamma_2. \tag{8}$$

For the system displayed in figure 7, measurements of the interfacial tensions give $\gamma_1 = 23.0 \pm 0.1\,\mathrm{mN\,m^{-1}}$, $\gamma_2 = 20.6 \pm 0.1\,\mathrm{mN\,m^{-1}}$ and $\gamma_{12} = 1.6 \pm 0.3\,\mathrm{mN\,m^{-1}}$, which gives as a driving tension: $\Delta\gamma = 4.0 \pm 0.5\,\mathrm{mN\,m^{-1}}$. The latter value is in good agreement with a direct measurement of the force (by the tilting method), which yields $F/2\pi R = 4.1 \pm 0.4\,\mathrm{mN\,m^{-1}}$. This value is rather low (in spite of the action of the intermediate meniscus, which now favours the motion), because the condition of complete wetting imposes the use of liquids of small surface tensions, which lowers the contrast between γ_1 and γ_2.

2.5. *Miscible liquids*

Bislug experiments might also be realized with miscible wetting liquids. The motion should exist, provided the liquids have different surface tensions. Then, the force per unit length can simply be written:

$$\Delta\gamma = \gamma_1 - \gamma_2. \tag{9}$$

The experiment can be achieved, for example, by juxtaposing toluene ($\gamma_1 = 28.5\,\mathrm{mN\,m^{-1}}$) and silicone oil ($\gamma_2 = 20.6\,\mathrm{mN\,m^{-1}}$) in a tube. As long as the two liquids are not completely mixed, the slug is asymmetric and moves (figure 8). The slug typically moves on its own length and stops when the mixture becomes uniform. Thus, this system should be relevant for applications where the movement is limited.

The mixing can be limited by introducing an air bubble as a spacer between the liquids. Then, the system remains asymmetric much longer, which keeps the motion alive (figure 9).

https://doi.org/10.1017/S0022112002000126X Published online by Cambridge University Press

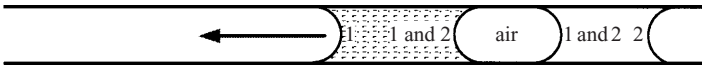


FIGURE 9. An air bubble as a spacer between the two miscible liquids slows down the mixing.

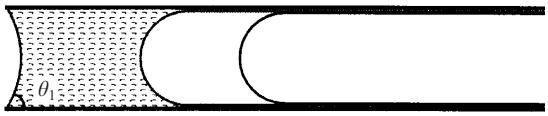


FIGURE 10. Bislug at the end of the tube. The value of the contact angle fits a Laplace pressure balance.

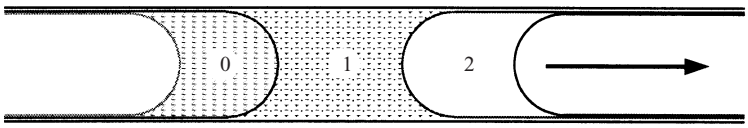


FIGURE 11. Reverse motion: juxtaposing a liquid of low surface tension can invert the motion.

2.6. *Reversing the motion*

As it moves, the bislug can finally reach the end of the tube. The front meniscus is pinned at the tube end and the contact angle at that place is allowed to take any value between 0° and 90°. It indeed increases, up to the point where Laplace pressures are balanced (figure 10). The equilibrium contact angle θ_1 is then given by $\gamma_1 \cos\theta_1 = \gamma_{12} + \gamma_2$.

If an index of a liquid 0 of low surface tension (for example hexadimethylsiloxane, the lightest silicone oil, if considering the system ethylene glycol/viscous silicone oil) is juxtaposed to the train, a *trislug* forms and starts flowing towards the opposite direction (figure 11). The driving interfacial tension now is:

$$\Delta\gamma = \gamma_2 + \gamma_{12} - \gamma_{10} - \gamma_0, \tag{10}$$

where γ_0 is the surface tension of the third liquid and γ_{10} its interfacial tension with liquid 1. In the system we described, the values of the different tensions are respectively 20.3, 18, 16 and 4.3 mN m^{-1}, which leads to a driving tension of 18 mN m^{-1}.

3. Dynamics

3.1. *Observations*

The experiment consists in introducing a bislug in a horizontal capillary tube and monitoring the position x of the front as a function of time. The results displayed in figure 12 correspond to an ethylene glycol/silicone oil drop in a millimetric tube first prewetted with a film of ethylene glycol of thickness 4 μm. The velocity is a constant (of the order of 1.5 mm s^{-1} in this example), although the length of the bislug decreases slightly (less than 10%), because of the coating.

We first focus on the case where the two liquids have comparable viscosities and study how the bislug speed varies as a function of its length, its viscosity and the tube radius.

3.2. *Long trains*

We first neglect dissipations close to the contact lines (case of long trains) and consider liquids of comparable viscosities. Then, balancing the driving force F with

https://doi.org/10.1017/S002211200200126X Published online by Cambridge University Press

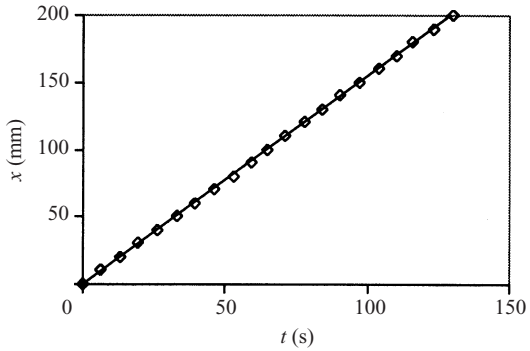


FIGURE 12. Position of an ethylene glycol/silicone oil bislug as a function of time. The glass tube radius is 341 μm and the successive lengths are 16 mm and 11 mm. The two liquids have the same viscosity of 17 mPa s. The velocity is observed to be a constant, equal to 1.55 mm s^{-1}.

the Poiseuille friction inside the train, we can write,

$$F = 8\pi(\eta_1 l_1 + \eta_2 l_2)V, \tag{11}$$

where V is the bislug speed, η_1 and l_1 the viscosities and the lengths of both parts (as soon as l_1 is centimetric, the meniscus size can be neglected). We thus find a constant velocity for the train:

$$V = \frac{R\Delta\gamma}{4(\eta_1 l_1 + \eta_2 l_2)}. \tag{12}$$

If both liquids have the same viscosity η, the velocity simply reduces to (Bico & Quéré 2000):

$$V = \frac{R\Delta\gamma}{4\eta L}, \tag{13}$$

where L is the total length of the bislug.

Figure 13 shows the train velocity as a function of its length for the system ethylene glycol/silicone oil in a prewetted glass tube of radius $R = 341$ μm. The viscosity of both liquids is 17.3 ± 0.5 mPa s and the driving tension $\Delta\gamma$ was shown in the previous section to be 10 mN m^{-1}. The results are described well by equation (13) if the bislug is long ($L > 5$ cm). For shorter trains, the dissipation in the menisci cannot be neglected, which implies smaller velocities, as observed. We describe this additional friction in the next section.

A second series of experiments was carried out with an ethanol/silicone oil train in a dry tube of polyethylene (the middle meniscus is inverted, system displayed in figure 7). The driving interfacial tension is 4.1 mN m^{-1} and the tube radius is 425 μm. Since the viscosities of the two liquids are not the same (respectively, 1.45 mPa s and 17 mPa s), the length of the ethanol index is kept constant ($l_1 = 13$ mm) and the bislug speed measured as a function of l_2, the length of the oil index. The measured velocities are plotted in figure 14 and compared with the Poiseuille model (equation (12)). The data are found to deviate dramatically from this prediction, which confirms the hypothesis of an additional dissipation, which is enhanced here by the fact that two menisci are moving on a dry solid.

3.3. *Local dissipations*

The motion of a meniscus on a solid surface has been a subject of large interest and controversy for the past three decades. The tricky point relies on the application of the

https://doi.org/10.1017/S0022112002001260X Published online by Cambridge University Press

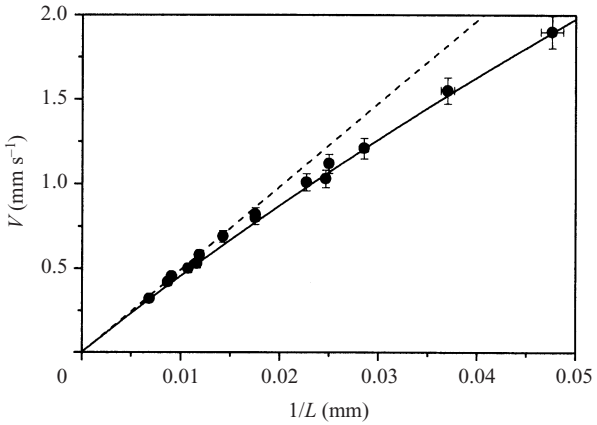


FIGURE 13. Speed of an ethylene glycol/silicone oil bislug as a function of its length. The data are compared with equation (13) (dotted line) and with equation (21) (solid line).

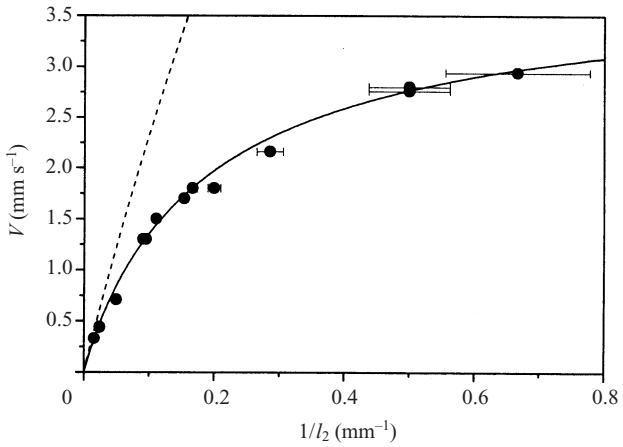


FIGURE 14. Velocity of an ethanol/silicone oil bislug in a dry polyethylene tube of radius 425 μm with an ethanol index of constant length (13 mm). The data are compared with equation (12) (dotted line) and with a model taking into account additional dissipation in the menisci (equation (21), solid line).

non-slip condition close to the contact line. However, the relevant physical ingredients of this problem are commonly admitted: viscous friction tends to retain the liquid at the vicinity of the tube wall while capillarity tries to restore the static shape of the meniscus. This dynamic effect flattens an advancing meniscus and increases the curvature of a receding one (figure 15). Neglecting inertia, the dynamic advancing contact angle is a function of the capillary number Ca, the quantity which compares viscous and capillary forces:

$$Ca = \frac{\eta V}{\gamma}. \tag{14}$$

Measurements of dynamic contact angles θ in capillary tubes have been conducted by Hoffman (1975), who showed that θ scales as $Ca^{1/3}$, for θ in the interval $[0°, 120°]$. A straightforward argument due to de Gennes (1985) explains this law for small θ: balancing the non-compensated capillary force with the viscous force close to the

https://doi.org/10.1017/S0022112002000126X Published online by Cambridge University Press

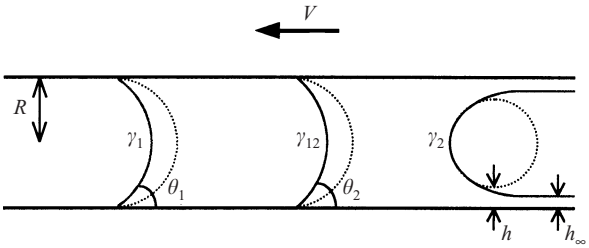


FIGURE 15. Dynamic contact angles and film coating in a moving bislug (the middle meniscus here is inverted, i.e. it faces the front).

contact line leads to:

$$\theta = \left(6\Gamma \frac{\eta V}{\gamma}\right)^{1/3}, \tag{15}$$

where the prefactor Γ is related to physical cutoffs, typically the tube radius R and a molecular length a, in the expression of the viscous dissipation:

$$\Gamma = \ln(R/a). \tag{16}$$

If the tube radius is in the millimetre range and a of the order of some angstroms, Γ is about 15. Such a value in equation (15) provides an excellent agreement with Hoffman's data.

The thickness h_∞ of the film deposited behind a wetting meniscus is also a function of the capillary number Ca (Bretherton 1961; Taylor 1961), since viscosity and capillarity play antagonist roles in this process (viscosity causes the deposition while capillary forces oppose the formation of a film). Here again, the resolution of this problem leads to a simple scaling law (Bretherton 1961):

$$h_\infty = 1.34 R Ca^{2/3}, \tag{17}$$

where h_∞ is the final thickness of the coating film. This relation is valid in the range $10^{-5} < Ca < 10^{-2}$. Van der Waals forces become important for very thin films (low value of Ca), as shown by Teletzke (1983) and Joanny (1985). Conversely, the limit for the film thickness at high capillary numbers was described by Taylor (1961).

If we consider a bislug with an inverted middle meniscus, the curvature of the three menisci is affected by the liquid flow (figure 15): the two first driving menisci are flattened, while the curvature of the third one becomes higher because of the deposition of a coating film.

These three dynamic effects tend to slow down the bislug, whose driving pressure becomes:

$$\Delta P_m = \frac{2\gamma_1 \cos\theta_1}{R} + \frac{2\gamma_{12}\cos\theta_2}{R} - \frac{2\gamma_2}{R-h}, \tag{18}$$

where θ_1 and θ_2 are the dynamic contact angles at the first and second meniscus and h is the difference between the actual radius of the third meniscus and the tube radius. Bretherton showed that it is simply proportional to h_∞ the thickness of the deposited film ($h = 2.90\, h_\infty$). Using equations (17) and (15), and expanding for small Ca, we obtain:

$$\Delta P_m = \frac{2\Delta\gamma}{R}\left(1 - \left(\frac{V}{V^*}\right)^{2/3}\right). \tag{19}$$

$\Delta\gamma$ is the driving interfacial tension $\Delta\gamma = \gamma_1 + \gamma_{12} - \gamma_2$, and the characteristic speed

https://doi.org/10.1017/S002211200200126X Published online by Cambridge University Press

V^* is defined as:

$$V^* = \left(\frac{\Delta\gamma}{1.65\Gamma^{2/3}(\gamma_1^{1/3}\eta_1^{2/3} + \gamma_{12}^{1/3}\eta_2^{2/3}) + 3.88\gamma_2^{1/3}\eta_2^{2/3}} \right)^{3/2}. \tag{20}$$

The speed of the train is finally deduced from a balance between the Poiseuille pressure drop, (11), with the dynamic driving pressure, (19), which gives:

$$V = \frac{R\Delta\gamma}{4(\eta_1 l_1 + \eta_2 l_2)} \left(1 - \left(\frac{V}{V^*} \right)^{2/3} \right). \tag{21}$$

Equation (21) shows that V^* is the maximum possible velocity of the bislug. Since it is fixed by local dissipations, it is logically found to be independent of the tube radius (neglecting the only logarithmic dependence contained in Γ). For the system ethanol/silicone oil ($\gamma_1 = 23\,\mathrm{mN\,m^{-1}}$, $\gamma_{12} = 1.6\,\mathrm{mN\,m^{-1}}$, $\gamma_2 = 20.6\,\mathrm{mN\,m^{-1}}$, $\eta_1 = 1.45\,\mathrm{mPa\,s}$, $\eta_2 = 17\,\mathrm{mPa\,s}$ and $\Gamma = 15$), we find $V^* = 5\,\mathrm{mm\,s^{-1}}$. In the limit of long trains ($V \to 0$), equation (21) reduces to the Poiseuille expression (equation (12)), the local dissipative effects being in this limit dominated by the bulk dissipation. Equation (21) can finally be drawn and compared with the data, see figure 14.

Equation (21) can also be adapted to the first case described here, where the middle meniscus was opposing the motion and where the tube was first prewetted by a film of liquid 1. Equation (21) is indeed found to fit the data in figure 13, taking for the characteristic velocity $V^* = 23\,\mathrm{mm\,s^{-1}}$. This value is larger than in the previous example, in particular, because of the existence of a prewetting film. Then, the friction is attenuated, which can be treated by taking the thickness of this film as a small cutoff in the factor Γ (Joanny 1985):

$$\Gamma \approx \ln(R/h_p), \tag{22}$$

where h_p is the thickness of the prewetting film. This thickness was measured (by considering the shortening of the index of liquid 1 first moved to prewet the tube) and found to be $5\,\mu\mathrm{m}$. As the tube radius is $341\,\mu\mathrm{m}$, Γ should be of order 4. Using Bretherton's law, (17), to estimate the two rear menisci, the expression for V^* becomes:

$$V^* = \frac{1}{\eta} \left(\frac{\Delta\gamma}{1.65\Gamma^{2/3}\gamma_1^{1/3} + 3.88(\gamma_{12}^{1/3} + \gamma_2^{1/3})} \right)^{3/2}. \tag{23}$$

The measured values of the interfacial tensions and the viscosities give $V^* = 16\,\mathrm{mm\,s^{-1}}$, in fair agreement with the value deduced from the fit.

The modest values of the maximum speed V^* might be frustrating for practical applications such as driving liquid fuels in a low-gravity environment. However, much higher speeds can be reached with liquids of lower viscosity presenting a large contrast in surface tensions. Velocities as large as $1\,\mathrm{m\,s^{-1}}$ have, for instance, been measured for a centimetric bislug composed of water and ether ($\gamma_1 = 72\,\mathrm{mN\,m^{-1}}$, $\gamma_2 = 16\,\mathrm{mN\,m^{-1}}$ and $\gamma_{12} = 11\,\mathrm{mN\,m^{-1}}$).

4. Self-lubrication

4.1. *Principle*

We now focus on the possibility of tuning the contrast between the viscosities of both liquids. Systems composed of ethylene glycol and silicone oil have been selected

https://doi.org/10.1017/S002211200200126X Published online by Cambridge University Press

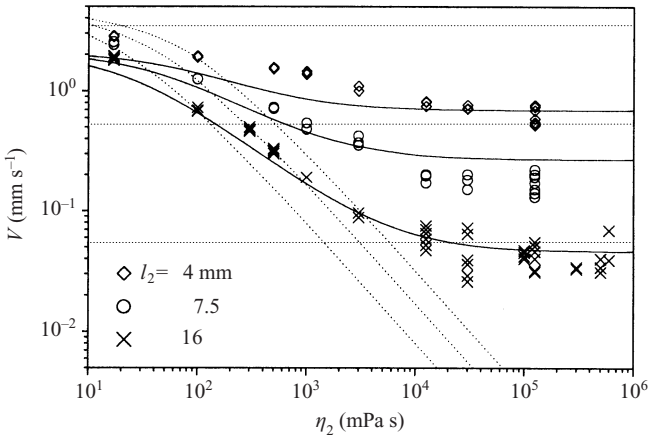


FIGURE 16. Train velocity as a function of the viscosity of the oil composing the waggon, for three different waggon lengths. The data are compared with a Poiseuille model (equation (12), dotted line), a plateau velocity calculated from a first-order self-lubricating model (equation (29), horizontal dashed line) and a model taking into account additional dissipations developed in the Appendix (solid line).

for this purpose. The polymeric oils are available in a large range of viscosities (from 17 mPa s to 60×10^5 mPa s) and provide interfacial tensions independent of the viscosity. We confirmed this fact by measuring the driving interfacial tension, and found constantly $\Delta\gamma \approx 10\,\mathrm{mN\,m^{-1}}$.

The series of experiments consisted of measuring the velocity with a fixed locomotive, and varying the viscosity of the trailing slug, or waggon. After a transient regime during which the bislug typically moves on the oil length, a steady speed was observed. Surprisingly, this velocity remains relatively high (of order of a fraction of mm s^{-1}), even with the most viscous oils. These results are displayed in figure 16, where the bislug velocity is plotted versus the oil viscosity, for three different lengths of oil index and a given length of ethylene glycol length (15 ± 1 mm). The tube has a radius of 0.511 mm and is prewetted with ethylene glycol before each experiment. For small oil viscosities η_2, the bislug speed decreases as η_2 increases, in qualitative agreement with the Poiseuille model, (12). But for highly viscous oils, the velocity deviates from the expected behaviour and reaches a plateau independent of the oil viscosity. The bislug can move much faster than predicted from the Poiseuille model, (12); for an oil viscosity of 10^5 mPa s, the speed is one thousand times higher than expected.

4.2. *Slipping cars*

The mobility of these trains is due to the self lubrication of the system; the trail left by the locomotive acts as a lubricant for the second (viscous) index, as sketched in figure 17. If the second liquid is very viscous compared with the first one, most of the viscous dissipation occurs in the lubricating film. A simple Couette flow is then expected, if the viscous stress is lower in the lubricant than it would be in the viscous oil without any lubrication. This condition is expressed as:

$$\frac{\eta_1 V}{h} \ll \frac{\eta_2 V}{R}. \tag{24}$$

https://doi.org/10.1017/S0022112002001260X Published online by Cambridge University Press

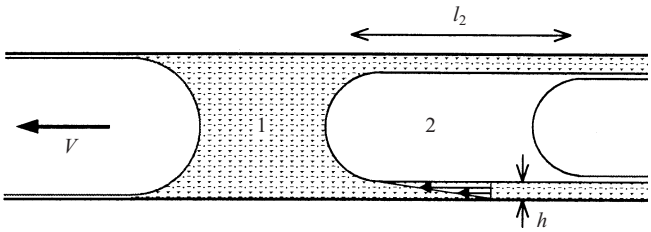


FIGURE 17. Self-lubrication: the second index can slip over the trail of the head index.

Then, the viscous force is given by (instead of equation (11)):

$$F = 2\pi R l_2 \frac{\eta_1 V}{h}, \tag{25}$$

where l_2 is the length of the waggon and h the thickness of the film deposited by the locomotive. Balancing this viscous force with the driving force, (2), yields:

$$V = \frac{h\Delta\gamma}{l_2\eta_2}. \tag{26}$$

As the film thickness also depends on the bislug speed, equation (26) is an implicit expression of the velocity. The value of h remains to be discussed. This problem is close to the Bretherton problem evoked earlier (equation (17)), but the film here is deposited in a highly viscous environment. Schwartz, Princen & Kiss (1986) derived the fluid flow equations with this particular condition ($\eta_2 \gg \eta_1$) and established that the thickness of the deposited film still obeys the Bretherton scaling, with a modified prefactor. The film is found to be thicker, by a factor $2^{2/3}$ (about 1.6). The thickening physically comes from the fact that the capillary backflow, which limits the film thickness, is less efficient than in the Bretherton problem, because of the presence of a very viscous liquid around. The Schwartz–Bretherton expression for the film thickness is finally written:

$$h = 2.13 R\, Ca^{2/3} \quad \text{with} \quad Ca = \eta_1 V/\gamma_{12}. \tag{27}$$

It is worth checking the validity of this expression. We measured the film thickness by observing the shortening of the first index during the motion of the bislug (which could be either spontaneous or forced by a slope, to vary the speed more conveniently). The flow conservation leads to the following relation between these two quantities:

$$h = R\frac{\Delta l_1}{x}, \tag{28}$$

where Δl_1 is the shortening of the first index for a displacement x of the bislug. This relation is only valid if we have $\eta_2/\eta_1 \gg R/h$. A more accurate derivation presented in the Appendix was used for our measurements.

The results are plotted in figure 18 as a function of the capillary number. The film is found to be significantly thicker than a Bretherton film, and the data are well described by the Schwartz–Bretherton equation, (27).

We can now express explicitly the velocity in equation (26), using equation (27) (Bico & Quéré 2000). We find:

$$V = 9.62\frac{\Delta\gamma}{\eta_1}\left(\frac{\Delta\gamma}{\gamma_{12}}\right)^2\left(\frac{R}{l_2}\right)^3. \tag{29}$$

https://doi.org/10.1017/S002211200200126X Published online by Cambridge University Press

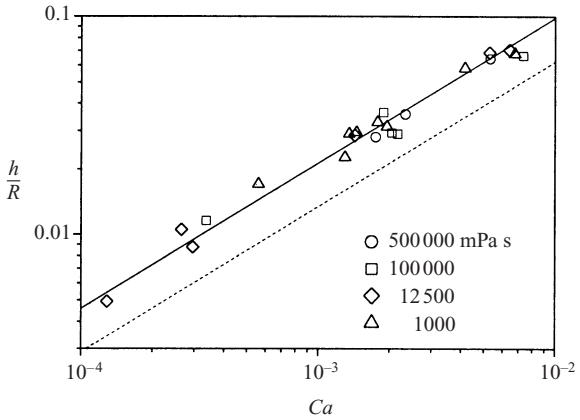


FIGURE 18. Lubricant film thickness measured for different oil viscosities and compared with the Schwartz–Bretherton law (equation (27), solid line) and with the Bretherton law (equation (17), dotted line).

The lubrication condition, (24), is finally written as:

$$\eta_2 \gg 0.1\eta_1 \left(\frac{\gamma_{12} l_2}{\Delta\gamma R}\right)^2. \tag{30}$$

Equation (29) is independent of η_2, the viscosity of the second index, in agreement with the observations in figure 16, where it is represented by a dotted line. A quantitative agreement is found for the longest bislug ($l_2 = 16\,\text{mm}$). For shorter waggons, the experimental speeds are significantly lower than predicted. Viscous dissipation in the first index and the dynamic curvatures of the menisci have been neglected in this first approach. These additional dissipations are relatively important for shorter indices and must be taken into account for a better description of the flow.

4.3. *Additional dissipations*

The flow in the head index induces a Poiseuille force which is written as:

$$F = 8\pi_1 l_1 \eta_1 V. \tag{31}$$

However, as stressed above, most of the additional occurs in the contact lines, which reduces the driving interfacial tension $\Delta\gamma$ of a factor $[1-(V/V^*)^{2/3}]$, as described in equation (19). The characteristic speed V^* is given by equation (23), slightly adapted to this particular situation:

(i) The expression for the advancing meniscus curvature remains the same; with a Γ-value corresponding to a prewetted tube ($\Gamma \approx 4$–5).

(ii) The lubricant thickness is now given by the Schwartz–Bretherton law, (27), so that the prefactor 3.88 must be multiplied by $2^{2/3}$.

(iii) The very slight diminution of the second index length during its displacement shows that the second coating film is very thin (this problem of double coating is developed in § 5). Thus, we assume the same curvature for both the rear and the middle menisci.

If we take into account these modifications, the expression of the speed V^* becomes:

$$V^* = \frac{1}{\eta_1}\left[\frac{\Delta\gamma}{1.65\Gamma^{2/3}\gamma_1^{1/3} + 12\gamma_{12}^{1/3}}\right]^{3/2}. \tag{32}$$

https://doi.org/10.1017/S0022112002001260 Published online by Cambridge University Press

For an ethylene glycol/silicone oil system, this gives $V^* = 5\,\mathrm{mm\,s^{-1}}$. The introduction of both additional dissipations finally leads to the expression of the speed:

$$V = \frac{\Delta\gamma}{\eta_1}\frac{R}{l_2}\frac{1-\left(\dfrac{V}{V^*}\right)^{2/3}}{\left(\dfrac{\gamma_{12}}{3.1\eta_1 V}\right)^{2/3}+\dfrac{l_1}{l_2}}. \tag{33}$$

The solutions of this equation for the oil lenths 4, 7.5 and 16 mm are, respectively, 0.69, 0.27 and $0.045\,\mathrm{mm\,s^{-1}}$, which are much closer to the experimental data (respectively, 0.6, 0.2 and $0.05\,\mathrm{mm\,s^{-1}}$). A complete description of the transition from the Poiseuille regime to the self-lubricating plateau is developed in the Appendix. The dissipation in the second liquid (which depends on η_2) is taken into account in this model which fits the experimental results in figure 16 well, whatever the oil viscosity or the index length.

5. Double coating

In this section, we focus on the double trail left behind a 'classical' bislug (when the middle meniscus is inverted as in figure 7, a single film is deposited and its thickness is given by the Bretherton law, (17)). We discussed the law for the deposition of the first film, and how it is modified by the presence of a surrounding viscous fluid (equation (27)). The problem is much more complex for the second film, which is deposited on a liquid, which lubricates the deposition. Our main aim here is to show experimentally how the presence of a liquid below the deposited film affects the film thickness. Then, we discuss the possible formation of lobes at the rear of the drop, which can stop the motion.

5.1. *Measurements*

The thickness h_2 of the second film is deduced from the shortening of the second index. To vary conveniently the speed of deposition, the tube was tilted, which adds gravity as a driving force for the bislug and allowed us to achieve speeds between 0.1 and $10\,\mathrm{mm\,s^{-1}}$. Long capillary tubes of 50 cm were used to improve the sensitivity of the experiment. The index length was measured with a camera fitted with a macro lens, which gives an accuracy on the index length of 0.1 mm. This yields a precision for the film thickness of the order of $10^{-4}R$ (less than 0.1 μm). The systems studied are the same as in the previous section: ethylene glycol index followed by silicone oil, whose viscosity can be tuned between 17 mPa s and 500 000 mPa s. The ratio h_2/R obtained from several series of experiments is plotted in figure 19 as a function of the capillary number $Ca_2 = \eta_2 V/\gamma_2$.

The thickness of the Bretherton film is also indicated in figure 19, and the second film is found to be much thinner. In addition, it is observed that h_2 decreases with Ca, for high capillary numbers. Both features are related to the deposition of the first liquid which reduces the friction, and thus the film thickness h_2. The lubricant thickness increases with the velocity (see figure 18), which induces a reduction of the second coating.

5.2. *Slipping length*

The thickness of the lubricant film was found to obey the Schwartz–Bretherton law, (27). We can define for the second liquid moving on this film a slipping length b,

https://doi.org/10.1017/S002211200200126X Published online by Cambridge University Press

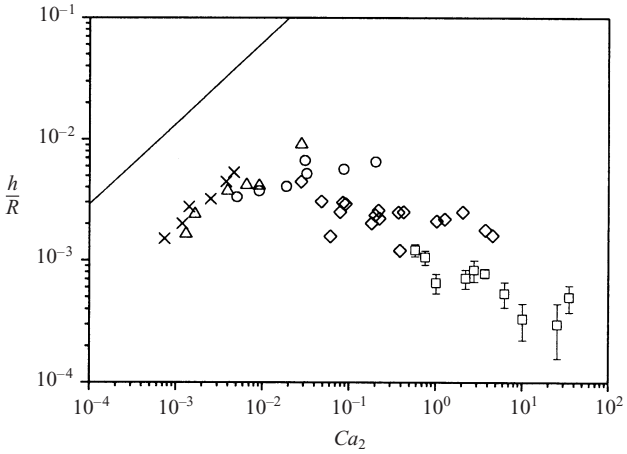


FIGURE 19. Ratio h_2/R as a function of the capillary number $Ca_2 = \eta_2 V/\gamma_2$ for different oil viscosities: ×, 17 mPa s; △, 100 mPa s; ○, 1000 mPa s; ◇, 12 500 mPa s; □, 100 000 mPa s. The Bretherton law (equation (17)) is the solid line.

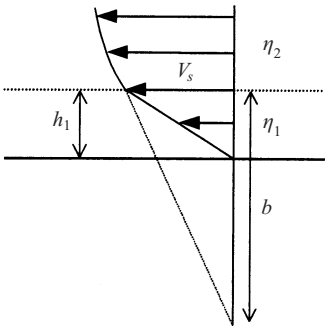


FIGURE 20. Definition of the slipping length b for the second liquid.

defined as the virtual distance for which the extrapolated velocity profile vanishes (figure 20). The stress continuity condition gives:

$$\eta_2 \frac{V_s}{b} = \eta_1 \frac{V_s}{h_1}, \tag{34}$$

where V_s is the fluid velocity at the liquid–liquid interface and h_1 the lubricant thickness. This expression should only be relevant when the viscosity is much higher for the second liquid than for the first one (which can then play the role of a lubricant). The introduction of the Schwartz–Bretherton law, (27), leads to:

$$b = 2.13R\frac{\eta_2}{\eta_1}\left(\frac{\eta_1 V}{\gamma_{12}}\right)^{2/3}. \tag{35}$$

We propose to look for deviations towards the Bretherton law by expressing the results in the following way:

$$h_2 = 1.34R\,P(b/R)Ca_2^{2/3}, \tag{36}$$

where the prefactor $P(b/R)$ is expected to tend towards unity when the slipping length vanishes. This quantity can be deduced from experiments such as those reported in

https://doi.org/10.1017/S002211200200126X Published online by Cambridge University Press

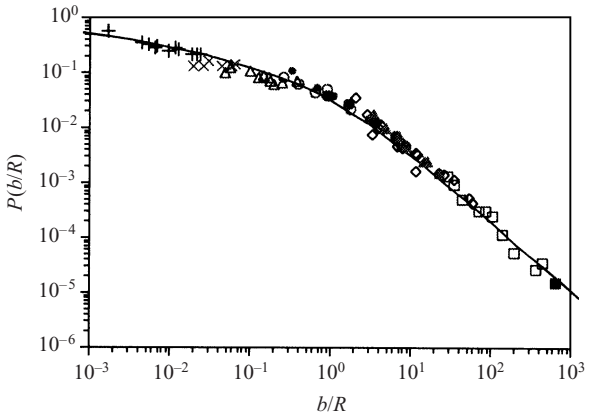


FIGURE 21. Experimental measurement of the factor $P(b/R)$ (ratio of the thickness over that of Bretherton, as defined in equation (36)) as a function of the normalized slipping length b/R for different oil viscosities and tube radii: +, 5 mPa s; ×, 16 mPa s; △, 100 mPa s; ○, 1000 mPa s; ◇, 12 500 mPa s; □, 100 000 mPa s; and ■, 500 000 mPa s in a tube of radius 341 μm; 1000 mPa s in a tube •, of radius 250 μm; or ●, 984 μm; surfactant solution (dTAB at 10 cmc) and silicone oil of 1000 mPa s in ▲, a tube of 341 μm. Straight line: empirical fit given by equation (37).

figure 19, and for each experiment b can be estimated from equation (35). Figure 21 shows the way they depend on each other. The data are taken from figure 19, and additional experiments are superimposed; as another kind of bislug (to test the influence of (γ_2), we chose a surfactant solution (*n*-decyltrimethyl ammonium bromide) of very high concentration (660 mmol l^{-1}, i.e. 10 times the c.m.c.), which allows us to limit Marangoni effects (Quéré & de Ryck 1998).

It turns out that this representation makes all the experimental data collapse on the same master curve. This curve is correctly fitted by the empirical expression:

$$P(b/R) \approx \frac{1}{1 + 15(b/R)^{0.4} + 17(b/R)^{1.25}}, \tag{37}$$

also represented in figure 21. Equations (36) and (37) allow us to propose an empirical relation for the thickness of the second film:

$$h^* \approx \frac{1.34R(Ca^*)^{2/3}}{1 + 18(Ca^*)^{0.27} + 32(Ca^*)^{0.83}}, \tag{38}$$

with

$$h^* = \left(\frac{\gamma_2}{\gamma_1}\frac{\eta_2}{\eta_1}\right)^{2/3} h_2, \quad Ca^* = \left(\frac{\eta_2}{\eta_1}\right)^{3/2}\left(\frac{\eta_1 V}{\gamma_{12}}\right).$$

The latter expression allows us to describe the experimental data quite well, as shown in figure 22. Nevertheless, this study remains empirical and must be further implemented by theoretical arguments or numerical simulations.

5.3. *Formation of lobes*

We saw that a bislug in a wetting situation moves under the action a well-defined force. It leaves (in the most usual situation) two films, of thicknesses given by equations (27) (or possibly (17)) and (38). However, a special case can complicate these views. Let us consider a bislug composed of ethylene glycol (liquid 1) and toluene (liquid 2) juxtaposed in a glass tube. Interfacial tensions γ_1, γ_{12} and γ_2 are, respectively, 47.7,

https://doi.org/10.1017/S002211200200126X Published online by Cambridge University Press

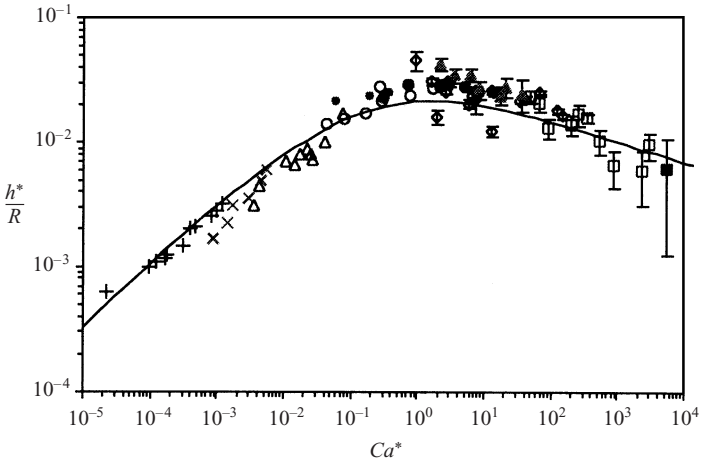


FIGURE 22. Normalized thickness h^* as a function of the capillary number Ca^* defined by (38); same symbols as in figure 21. The solid line corresponds to equation (38).

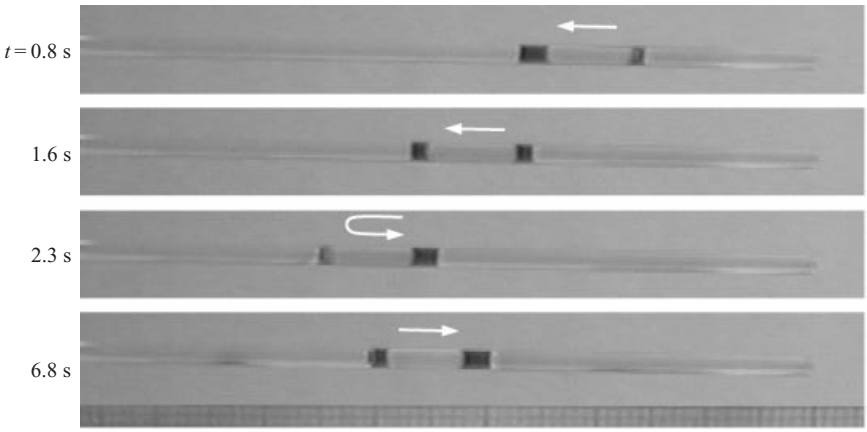


FIGURE 23. Ethylene glycol/toluene bislug in a glass tube (for a better visualization, the ethylene glycol index has been dyed).

8.9 and 28.3 mN m^{-1}, which leads to a positive driving tension $\Delta\gamma$ of 10.5 mN m^{-1}. The bislug moves spontaneously, as expected, but a lobe appears and grows up near the rear meniscus (figure 23). The lobe finally pinches across the tube, and forms a lens, adding a second and a third waggon for the train, respectively, made of liquid 1 and liquid 2 (the latter coming from the film deposited on liquid 1, which coats the lens as it is formed). At this point, the system is still asymmetric and the motion goes on. However, the fourth index is rather short (of the order of the tube radius), so that it quickly vanishes because of the coating. Then, the system becomes symmetric and the motion stops. Note that in the example presented in figure 23, the train is even observed to reverse its motion; the liquid lengths have been carefully chosen to induce a simultaneous vanishing of the ethylene glycol and the fourth toluene indices.

The steps of the formation of the lobes (and the resulting stop of the train) are sketched in figure 24. The lobe formation is reminiscent of the Rayleigh instability (Rayleigh 1879); a liquid cylinder or an annular film are not stable and adopt a regular undulating shape which reduces the surface energy of the system. The characteristic

https://doi.org/10.1017/S002211200200126X Published online by Cambridge University Press

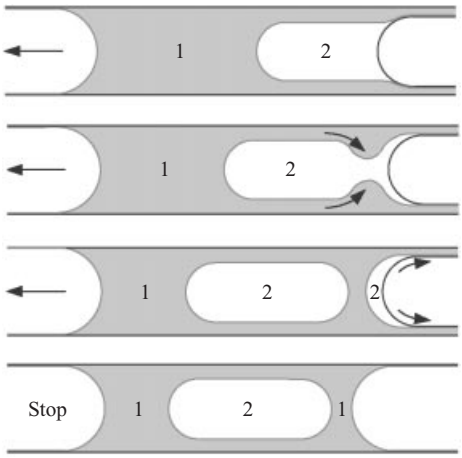


FIGURE 24. Formation of a lobe of liquid 1 at the rear meniscus which leads to the end of the motion.

wavelength of the fastest growing mode is given by the relation $\lambda = 2\sqrt{2}\pi R \approx 9R$, where R is the radius of the liquid cylinder. Long toluene indices would then lead to a string of lobes, which is not observed during the bislug motion. The difference between lobes and Rayleigh instability could be confirmed by the following experiment. A moving ethylene glycol/silicone oil bislug was stopped before the end of its trip by closing one end of the tube. The lubricant film then classically undergoes a Rayleigh instability, as expected. If the tube is reopened, the bislug starts again and the undulations are collected in a lobe at the rear meniscus. Contrary to the previous example, this Rayleigh-type lobe progressively disappears as the bislug moves.

The lubricant film is obviously responsible for the lobe instability. Its thickness is characterized by two limiting values figure 25: a first value h_1 between the tube wall and the waggon, and a second one h_1' in the trail of the bislug, where it is coated by a film of liquid 2. As detailed previously, h_1 can be estimated from a Bretherton-type law (equations (17) or (27)):

$$h_1 \sim R\left(\frac{\eta_1 V}{\gamma_{12}}\right)^{2/3}. \tag{39}$$

The value of the numerical prefactor is a function of the viscosity ratio and ranges between 1.34 and 2.13. If the second liquid is not too viscous compared with the first one, the value h_1' results from the same viscous dissipation as for h_1, but the capillary component should be related to the surface tension γ_2 (instead of γ_{12}). In a first approximation, the following scaling may be expected:

$$h_1' \sim R\left(\frac{\eta_1 V}{\gamma_2}\right)^{2/3}. \tag{40}$$

Because of flow conservation, a disproportionate thickness h_1 should lead to an accumulation of liquid near the rear meniscus. A condition for observing a lobe should thus be: $h_1' \ll h_1$, which yields:

$$\gamma_{12} \ll \gamma_2. \tag{41}$$

In the opposite case, the first flow is not important enough to supply the second flow and the thickness h_1' should be fixed by h_1. A more quantitative condition for the

https://doi.org/10.1017/S002211200200126X Published online by Cambridge University Press

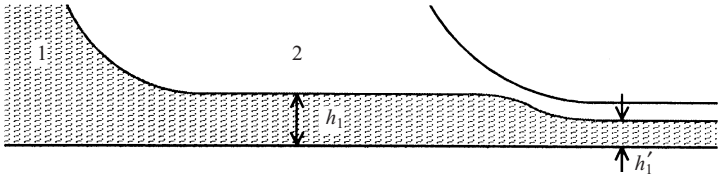


FIGURE 25. The two different thicknesses h_1 and h_1' of the lubricant film.

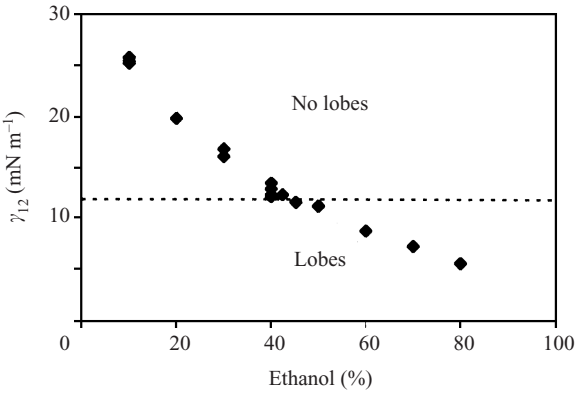


FIGURE 26. Interfacial tension γ_{12} between silicone oil and a solution of ethanol in water as a function of the ethanol concentration. When γ_{12} is below a critical value, a lobe grows up as the bislug moves.

onset of the lobe formation has been evaluated experimentally with a series of bislugs, where the first index consisted of a solution of ethanol in water and the second one of silicone oil. Varying the ethanol concentration allowed us to tune the interfacial surface tension γ_{12}, keeping γ_2 constant. Lobes appear, or not, and the corresponding results are plotted in figure 26, together with the measured variation of γ_{12} with the ethanol concentration.

A precise measurement of the critical value of the interfacial tension γ_{12} provides an empirical quantitative condition for the lobes formation:

$$\gamma_{12}/\gamma_2 < 0.6 \pm 0.1. \tag{42}$$

Other series of experiments have been carried out with squalane ($\gamma_2 = 28.5\,\mathrm{mN\,m^{-1}}$) or perfluorodecalin ($\gamma_2 = 16\,\mathrm{mN\,m^{-1}}$) and confirm this result. The system ethylene glycol/toluene has a ratio γ_{12}/γ_2 of order 0.3, and thus leads logically to the formation of lobes (figure 23). On the other hand, systems presented before this section do not satisfy criterion (42). For an ethylene glycol/silicone oil bislug, the ratio γ_{12}/γ_2 is 0.9 and lobes were not observed (figure 2).

Condition (42) remains empirical and theoretical improvements or flow simulations are necessary for a better description of the phenomenon, which is related to the complex double coating problem. This experiment shows anyway the uniquitous role of the lubricant; it allows highly viscous species to move in narrow environments, but it can also provoke this lobe instability, which opposes the motion of the train.

https://doi.org/10.1017/S002211200200126X Published online by Cambridge University Press



FIGURE 27. Spinning bislug.

6. Variations

We describe in this section different special bislugs, of potential interest for applications. We first present some experiments involving reactive liquids, which induce the manufacturing of polymer structures (tube coating or adjusted pistons) in a confined environment. Then, extensions to other geometries, from Hele-Shaw cells to simplified porous media, are discussed.

6.1. *Reactive systems*

All the systems presented until now were chemically inert and the motion was only due to the contrast between the interfaces. It would be nevertheless interesting to consider reactive systems which would eventually lead to the fabrication of small structures.

We start with a high school teaching experiment: the Nylon® synthesis. This polycondensation involves hexanediamine and adipoyl chloride (respectively, dissolved in water and in an organic solvent, such as chloroform). The reaction takes place at the interface between the two liquid phases. A polymeric film condenses at this interface, and a Nylon thread can be spun if the operator pulls out the product with a tip. In order to adapt this experiment to the liquid train system, an hexadiamine solution ($5\,\mathrm{mmol\,l^{-1}}$) in soapy water (sodium dodecyl sulfate at $8\,\mathrm{mmol\,l^{-1}}$) and a solution of adipoyl chloride in chloroform were juxtaposed in a capillary tube. A soapy water/chloroform train moves, but when the reactants are present, it does not because a polymer aggregate forms at the interface between both compounds and clogs the tube. To overcome this difficulty, we introduced an air bubble between both indices. Then, the water/air/solvent moves and the chemicals gently react in the films, so that a polymer film is deposited on the tube wall (figure 27). The thickness and the continuity of this film depend on the concentrations of the reactants and on the bislug speed and more experiments remain to be done to provide quantitative results.

6.2. *Special waggons*

6.2.1. *Running gels*

A variation on these spinning systems consists in inducing a reaction in the waggon. Light sensitive compounds ('poly 200' from Rhodia, a cross-linking polydimethylsiloxane compatible with silicone oils) were used for this purpose. A bislug composed of ethylene glycol and poly 200 spontaneously moves, leaving its trail behind. When a strong UV light is applied, the liquid in the trails cured and a solid coating of the tube is achieved (figure 28). If exposed to the light, the index of poly 200 can also solidify and the piston thus obtained perfectly fits the tube (the tolerance being controlled by the thin lubricant layer).

The same experiment can be reproduced with a mixture of silicone oil and poly 200 (in proportion 1:2) for the second index. The exposure of this index to UV light leads to the formation of a (solid) cylindrical gel plug within the tube. When such a piston is juxtaposed to an ethylene glycol index in a tube of the same size, this object spontaneously moves. The solid gel actually behaves as a spongy reservoir;

https://doi.org/10.1017/S002211200200126X Published online by Cambridge University Press

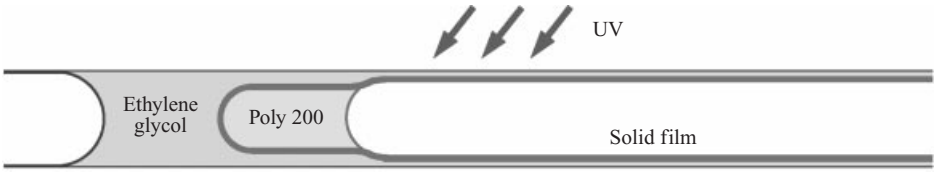


FIGURE 28. UV-cure on light sensitive film and index.



FIGURE 29. Running gel: a gel composed of a mixture of cross-linking silicone and inert silicone oil is juxtaposed to a first index of ethylene glycol. The observed spontaneous motion relies on the extraction of a film of silicone oil from the gel.



FIGURE 30. Motion of an encapsulated index *I*.

some silicone oil is released and coats the lubricant layer of the first liquid, which allows motion to occur (figure 29). This mechanism can be checked by measuring the driving force of this system, which was found to be the same as for a regular ethylene glycol/liquid silicone oil bislug. This proves the deposition of a film of silicone oil, which can only be provided by the gel. Since this film is very thin, such a bislug can move on long distances. The actual thickness of the film and the autonomy of this *running sponge* (de Gennes 1996) remain to be explored more quantitatively.

6.2.2. *Encapsulation of liquids*

An encapsulated liquid (let us say a toxic one) can be transported using a liquid train, as sketched in figure 30. However, because of the flow conservation, the driven index moves faster than its carrying liquid and a suitable length has to be evaluated to allow the train to reach a predefined target.

6.3. *Other geometries*

The extension of the bislug systems to other geometries can be problematic. For example, we did not succeed in achieving bislugs on flat substrates – one liquid immediately surrounds the other, and no translational motion is observed. On the other hand, bislugs can move in rectangular or square capillary tubes, or even in channels, which is of interest in microfluidics. We develop two other cases, in this section, namely, double rings in a Hele-Shaw cell, and trains in an irregular tube.

6.3.1. *Spontaneous burst of a double ring*

We first describe an experiment achieved in a Hele-Shaw cell. The experimental set-up is composed of two horizontal square glass planes ($10 \times 10\,\mathrm{cm}^2$), separated by microscope slides (thickness 1 mm). A hole (3 mm diameter) has been drilled at the centre of the upper plane. There, two concentric drops of ethylene glycol and silicone oil are introduced with a syringe (figure 31*a*). When some air is blown through the hole (bubble of radius r_2), the double ring formed spontaneously closes back if r_2 is small, but grows up and finally bursts if r_2 is large enough (figure 31*b*).

https://doi.org/10.1017/S002211200200126X Published online by Cambridge University Press

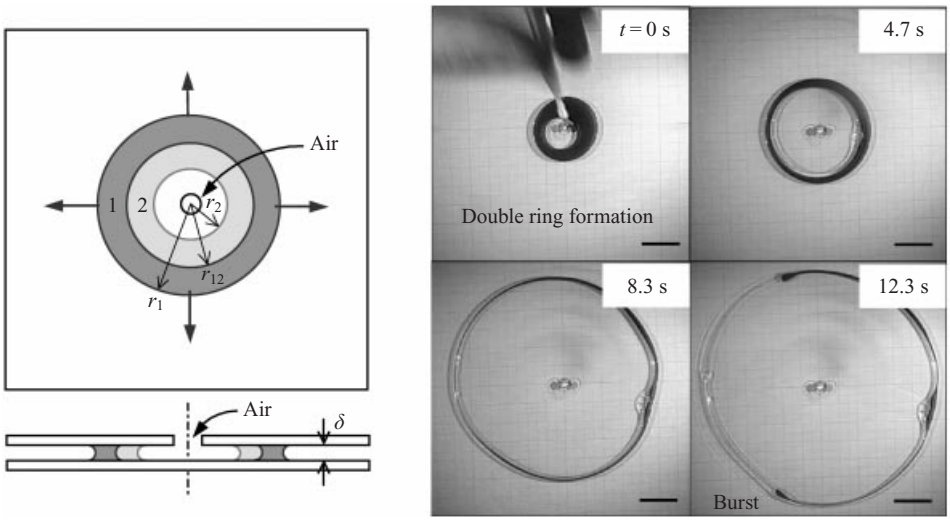


FIGURE 31. Hele-Shaw cell geometry. (*a*) Experimental set-up and double ring (upper and side views). (*b*) Spontaneous opening and burst of a double ring of ethylene glycol and silicone oil. The bar is 2 cm long.

The description of the dynamics of the double ring is rather technical and just relies on an adaptation to a cylindrical geometry of the relations derived in § 3 (Bico 2000). The expression of the driving pressure is nevertheless interesting since the critical hole size observed may remind us of the study by Taylor & Michael (1973) on the stability of a hole in a liquid sheet. Two types of curvature are present in this problem: the successive rings radii r_1, r_{12} and r_2 and the gap δ between the two plates. The Lapalace pressure difference between the inner and the outer radii is:

$$\Delta P = \frac{2\Delta\gamma}{\delta} - \frac{\gamma_1}{r_1} - \frac{\gamma_{12}}{r_{12}} - \frac{\gamma_2}{r_2} \quad \text{with} \quad \Delta\gamma = \gamma_1 - \gamma_{12} - \gamma_2. \tag{43}$$

The effect of the curvatures of the rings is to close back the system. Since their amplitudes are reduced when the hole becomes larger, the driving pressure $\Delta\gamma/\delta$ finally dominates, which leads to the extension of the double ring. The condition for opening is thus:

$$r_2 > \frac{\gamma_2}{2\Delta\gamma/\delta - \gamma_1/r_1 - \gamma_{12}/r_{12}}. \tag{44}$$

In the example of figure 31, r_1 and r_2 are initially 17 mm and 8 mm, which gives the minimum air disk radius $r_2 = 1.3$ mm. A larger disk such as that visible in figure 31(*b*), opens. Note, finally, the double ring growth does not lead to viscous fingering, as could happen in such a geometry (Saffman & Taylor 1958).

6.3.2. *Necks in tubes*

Porous materials are present in our daily life (paper, concrete materials, granular media), and the application of the bislug system to this complex geometry would be very interesting. We may, for example, imagine coating the surface in pores concrete (without clogging them) with a hydrophobic substance in order to achieve a water-repellent breathing material. Capillary tubes or Hele-Shaw cells are commonly used to model porous media, the tube diameter or the gap of the cell being related to a characteristic pore size. However, this pore size is not uniform in a real porous

https://doi.org/10.1017/S002211200200126X Published online by Cambridge University Press

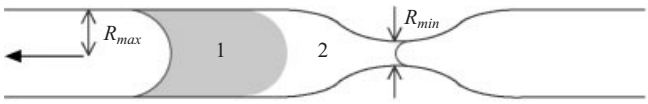


FIGURE 32. Rear meniscus blocked in a neck.

medium. Even if we restrict ourselves to the simple case of a tube with a neck (figure 32), one of the numerous features of a real porous medium, we understand that the motion of a bislug is not obvious. The rear meniscus may be blocked in the narrowest part of the tube, because of the large Laplace depression there (figure 32).

A necessary condition for overtaking this neck can be written:

$$\frac{\gamma_1 + \gamma_{12}}{R_{\max}} > \frac{\gamma_2}{R_{\min}}, \tag{45}$$

where $R_{\max}$ and $R_{\min}$ are the extreme radii of the tube. This condition can be rewritten as:

$$\frac{R_{\max}}{R_{\min}} < \frac{\gamma_1 + \gamma_{12}}{\gamma_2}, \tag{46}$$

which is rather restrictive, since it only allows a maximum ratio $R_{\max}/R_{\min}$ of the order of 2. The application of the bislugs to real porous networks thus appears problematic. On the other hand, local displacements (i.e. for which the ratio $R_{\max}/R_{\min}$ does not vary too much) could be described by bislug considerations, for triphasic systems confined in a porous medium.

7. Conclusion

When two liquid indices are juxtaposed in a capillary tube, the resulting bislug can move spontaneously. The driving force results from the surface tension contrast between the interfaces at the three menisci. A situation of total wetting for at least one meniscus is required for the motion, which provides a coating of the tube wall. The dynamics of these trains was then described. If the liquids have about the same viscosity, the driving force is balanced by a simple viscous dissipation (Poiseuille flow), which may be corrected by dynamic contact angle effects for short trains. Experiments carried out with a very viscous liquid for the second index exhibit self-lubricating properties; a film of the first liquid is deposited beween the second liquid and the tube wall, which lubricates a track for the viscous waggon. The train then moves at a reasonable speed in spite of the high viscosity of the trailing slug.

If the middle meniscus is turned towards the rear, the front slug leaves a film whose thickness was found to obey the classical Bretherton law, possibly corrected by a small numerical factor in the case of a very viscous waggon. This waggon also leaves a film, which leads to a double coating of the tube. The second film was observed to be much thinner than the first one and it does not thicken when increasing the speed of the bislug. The lubricant layer can also induce a lobe instability, in the vicinity of the rear meniscus, which leads to the encapsulation of the second index. A theoretical or numerical approach describing these results quantitatively remains to be done.

Potential applications of these liquid trains were also described, as systems involving reactive liquids, which can provide the formation of solid micro-structures inside the tube. Extensions to other geometries were finally considered. In a Hele-Shaw cell, for instance, double rings can spontaneously grow and burst. Application to porous

https://doi.org/10.1017/S002211200200126X Published online by Cambridge University Press

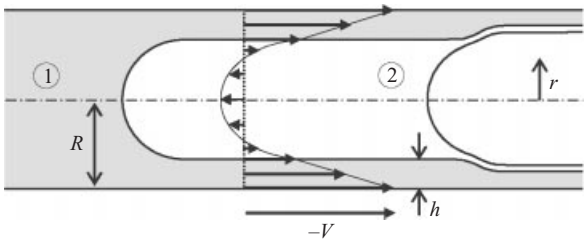


FIGURE 33. Coupled flow of the liquids in a lubricated index (the radial scale is largely amplified).

media would also be of great interest, but still remains a challenge (the liquid is usually blocked in the narrowest pores).

We thank J. Ashmore, P.-G. de Gennes, M. Deruelle, E. J. Hinch, D. Richard, H. Stone and W. Zhang for many discussions, suggestions and encouragement, and Rhodia for its financial support.

Appendix. Viscous dissipation in a lubricated index

Self-lubricating systems which involve two liquids with a very large contrast in viscosities have been described in § 3. The viscous liquid, which can slip on the film deposited by the first index, was somehow assumed to behave like a solid. This assumption greatly simplifies the description of the flow; the viscous stress relies on Couette flow in the lubricant film. However, since a very small strain in a highly viscous liquid can induce a huge viscous dissipation, the validity of this hypothesis must be carefully discussed.

Pressure gradient

In the following description the viscous index has been chosen as a reference in which the tube is moving at the speed $-V$ (figure 33). The pressure gradients only an axial component ∇P_2 (radial or angular flows from the ends of the index are neglected). The resolution of the Navier–Stokes equation in this cylindrical geometry gives as a general solution:

$$v_i(r) = -\frac{\nabla P_2}{4\eta_i} r^2 + A_i \ln\left(\frac{r}{R}\right) + B_i, \tag{A 1}$$

where v_i is the local velocity of the liquid i and η_i its viscosity. The constants A_i and B_i are fixed by the boundary conditions at the interfaces. The derivation of these constants does not require any difficulty and leads to:

$$A_1 = A_2 = 0, \quad B_1 = -\frac{\nabla P_2}{4\eta_1} R^2 - V, \quad B_2 = -\frac{\nabla P_2}{4\eta_1}(2Rh - h^2) + \frac{\nabla P_2}{4\eta_2}(R-h)^2 - V. \tag{A 2}$$

The pressure gradient ∇P_2 is finally deduced from the absence of global flow in the index:

$$\nabla P_2 = \frac{V}{(R-h)^2/8\eta_2 + (2Rh - h^2)/4\eta_1}. \tag{A 3}$$

This relation is compatible with equation (24) for the self-lubrication effect; the second liquid viscosity does not interfere if $R/h \ll \eta_2/\eta_1$.

https://doi.org/10.1017/S002211200200126X Published online by Cambridge University Press

Lubricant thickness

The flow rate q_1 of the lubricant liquid can be deduced from the previous relations:

$$q_1 = 2\pi V R^2 \left[\frac{(1-(1-\varepsilon)^2) - (1-(1-\varepsilon)^4)/2}{(1-\varepsilon)^2 \eta_1/\eta_2 + 2(2\varepsilon - \varepsilon^2)} - (1-(1-\varepsilon)^2)/2 \right], \qquad (A\,4)$$

noting $\varepsilon = h/R$. The flow rate can also be experimentally evaluated from the shortening ∇l of the first index length corresponding to a displacement x:

$$q_1 = -\pi R^2 V \frac{\Delta l}{x}. \qquad (A\,5)$$

Expanding (A 4) for small ε yields a simple relation for the lubricant thickness:

$$\left(\frac{h}{R}\right)^2 - \left(\frac{\Delta l}{x} - \frac{\eta_1}{2\eta_2}\right)\left(\frac{h}{R}\right) - \left(\frac{\eta_1}{\eta_2} - \frac{\Delta l}{x}\right) = 0. \qquad (A\,6)$$

Transition from Poiseuille to lubrication regimes

Equation (A 3) was used for the model curves drawn in solid line in figure 16, for describing the bislug velocity as a function of the viscosity of the second index. These curves were calculated from the balance of Laplace pressure (involving dynamic menisci) and the viscous dissipation in both indices:

$$\frac{2\Delta\gamma}{R} = \nabla P_1 l_1 + \nabla P_2 l_2, \qquad (A\,7)$$

where l_1 and l_2 are the lengths of the successive indices and the pressure gradient ∇P_1 is simply given by a Poiseuille law. An implicit expression for the speed cannot be deduced and such an equation has to be solved numerically, which gives the solid line in figure 16.

REFERENCES

Bain, C., Burnett-Hall, G. & Montgomerie, R. 1994 Rapid motion of liquid drops. *Nature* **372**, 414–415.

Bico, J. 2000 Mécanismes d'imprégnation: surfaces texturées, bigouttes, poreux. PhD thesis, University of Paris 6.

Bico, J. & Quéré, D. 2000 Liquid trains in a tube. *Europhys. Lett.* **51**, 546–550.

Bouasse, H. 1924 *Capillarité, phénomènes superficiels*. Delagrave, Paris.

Bretherton, F. P. 1961 The motion of long bubbles in tubes. *J. Fluid Mech.* **10**, 166–168.

Domingues dos Santos, F. & Ondarçuhu, T. 1995 Free running droplets. *Phys. Rev. Lett.* **75**, 2972–2976.

de Gennes, P. G. 1985 Wetting: statics and dynamics. *Rev. Mod. Phys.* **57**, 827–863.

de Gennes, P. G. 1996 Éponges filantes. *C R Acad. Sci. Paris* **323**, 663–667.

de Gennes, P. G. 1998 The dynamics of reactive wetting on solid surfaces. *Physica* A **249**, 196–205.

Hoffman, R. L. 1975 A study of the advancing interface. I. Interface shape in liquid gas systems. *J. Colloid Interface Sci.* **50**, 228–241.

Ichimura, K., Oh, S. K. & Nakagawa, M. 2000 Light driven motion of liquids on a photoresponsive surface. *Science* **288**, 1624–1626.

Joanny, J. F. 1985 Le Mouillage. PhD thesis, University of Paris 6.

Marangoni, C. 1871 Über die Ausbreitung der Tropfen einer Flüssigkeit auf Oberfläche einer anderen. *Ann. Phys. Chem.* **143**, 337–354.

Mazouchi, A. & Homsy, G. M. 2000 Thermocapillary migration of long bubbles in cylindrical capillary tubes. *Phys. Fluids* **12**, 542–549.

Quéré, D. & de Ryck, A. 1998 Le mouillage dynamique des fibres. *Ann. Phys.* **23**, 1–149.

Rayleigh, Lord 1879 On the stability of jets. *Proc. R. Soc. Lond.* A **10**, 4–13.

https://doi.org/10.1017/S002211200200126X Published online by Cambridge University Press

Saffman, P. G. & Taylor, G. I. 1958 The penetration of a fluid into a porous medium or Hele-Shaw cell containing a more viscous liquid. *Proc. R. Soc. Lond.* A **245**, 312–329.

Schwartz, L. W., Princen, H. M. & Kiss, A. D. 1986 On the motion of bubbles in capillary tubes. *J. Fluid Mech.* **172**, 259–275.

Taylor, G. I. 1961 Deposition of viscous fluid on the wall of a tube. *J. Fluid Mech.* **10**, 161–165 .

Taylor, G. I. & Michael, D. H. 1973 On making holes in a sheet of liquid. *J. Fluid Mech.* **58**, 625–641.

Teletzke, G. F. 1983 Thin liquid films, molecular theory and hydrodynamics implications. PhD thesis, University of Minnesota.

Weislogel, M. M. 1997 Steady spontaneous capillary flow in partially coated tubes. *AIChE J.* **43**, 645–655.

https://doi.org/10.1017/S002211200200126X Published online by Cambridge University Press